

Structure of Ribosomes of Chromatoid Bodies: Three-Dimensional Fourier Synthesis at Low Resolution

Abstract. A three-dimensional Fourier synthesis at an axial resolution of 75 angstroms of optical diffraction data from electron micrographs of stained sections of chromatoid bodies reveals the position of the large and small ribosomal subunits within these crystals of ribosomes.

The helical packing of the ribosomes within the crystal known as the chromatoid body has been described (1). Additional electron micrographs of longitudinal sections through such crystals have since been obtained (2) (see Fig. 1). The latter micrographs give a more detailed optical diffraction pattern than that of Morgan and Uzman (1) and show intensity on the 10th and 12th layer lines (Fig. 2). The 12th-layer line results from periodic structural detail within the micrograph of spacing 75 Å, and this spacing is, in effect, the resolution of the synthesis I describe. Using the mathematical technique for inverting such patterns given by Klug, Crick, and Wyckoff (3) and first used by De Rosier and Klug (4), I have calculated the distribution of electron density within one ribosome, which the data of Fig. 2 implies. A photograph of the

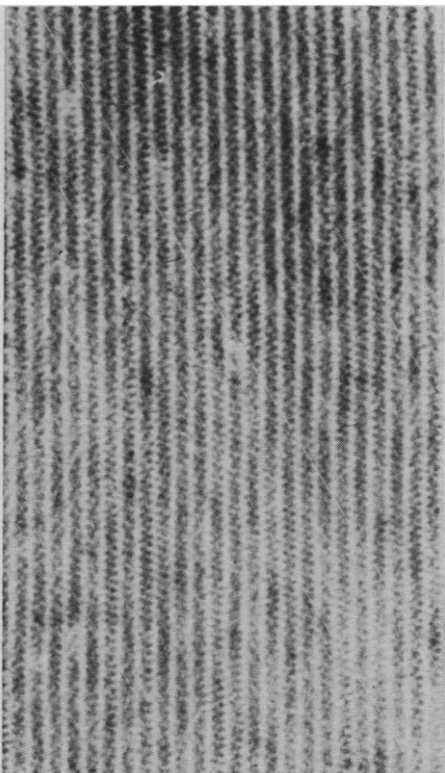


Fig. 1. Electron micrograph of a longitudinal section through a chromatoid body of *Entamoeba invadens*. The distance between neighboring chains is 440 Å (2).

overall shape of this result is shown in Fig. 3.

To perform this calculation, I have assumed that the pattern of Fig. 2 is the transform of a helix whose axial repeat consists of 12 nodes in 5 turns (1), each node being placed at a radius r_0 of 150 Å and having its mass concentrated at its center (1). In this case, the transform on any layer line l as a function of radius in diffraction space R has

$$G_{n,l}(R) = \sum_n J_n(2\pi R r_0)$$

where n and l are related by the helical selection rule (3). These G 's are all real numbers. [This symbolism is developed in reference (3), part 4]. Then, since successive values of n along any layer line are 12 apart, the summation over n reduces to the term with lowest n only. The diffracted intensity, $I(R)$, along layer lines 2, 3, 5, 10, and 12 of the pattern shown in Fig. 2 was measured with a Leeds and Northrup recording microdensitometer. The value for $G_{n,l}(R)$ was taken as $+ [I(R)]^{1/2}$, except for the second maximum of layer lines 5 and 12 which were taken as negative. The scale of I was arbitrary. Next I computed

$$g_{n,l}(r) = \sum_{i=0}^5 G_{n,l}(R_i) J_n(2\pi R_i r) 2\pi R_i$$

where $R_i = i \cdot 10^{-3}R$, for $r = 0, 50, 100, 150, 200, 250, \text{ and } 300$ Å. Finally I computed

$$\rho(r, \varphi, z) = \sum_{l=2}^{12} g_{n,l}(r) \cos(n\varphi - 2\pi lz/c)$$

for r at intervals of 50 Å from 0 to 300 Å, φ at intervals of 15° from -60° to +60°, and $z = 0, 25, 50, \text{ and } 75$ Å. The resulting values for ρ , together with the additional values generated by the helical symmetry, were plotted on polar coordinate paper for each z -level, and on rectangular coordinate paper for each value of φ . Contours of equal electron density were drawn. Templates were made of the shapes of the contours of zero electron density, both radially and horizontally, and these were assembled and covered to give the model ribosome shown in Fig. 3. The

model therefore represents the overall shape of a chromatoid body ribosome.

The striking feature emerging from these electron density maps is that each ribosome appears as two, clearly separated masses: one mass, two or three times the size of the other and white in the model, is centered at $r = 150$ Å, $\varphi = 0^\circ$, $z = 0$; the other mass, black in the model, is centered at $r = 75$ Å, $\varphi = -30^\circ$, $z = 75$ Å. The second mass is thus centered on the extension of the dyad axis which passes through the next ribosome up the helix. It seems entirely reasonable to suppose that the small or black part represents the small subunit of these ribosomes, which sediments at about 30S (5), and that the large or white part represents the large subunit, sedimenting at about 50S. The area of contact between them is small, being confined to the interval $r = 50$ to 150 Å, $\varphi = -15^\circ$ to $+15^\circ$, and $z = 50 \pm 10$ Å. Each subunit has a dyad axis (perpendicular to the helix axis) as an internal element of symmetry. This feature is a result of the fact that the model used for phasing this synthesis has this symmetry itself. It is not necessarily a feature of these ribosomes. In each subunit, the highest electron density is found at its center of mass. In this model, most of the large subunit can be contained by a rectangular box, 150 by 150 by 300 Å, and the smaller in one 100 by 100 by 150 Å. These dimensions are consistent with those derived for ribosomes by other techniques (6). When we place ribosomes of this shape on the chromatoid body helix, we find that the small

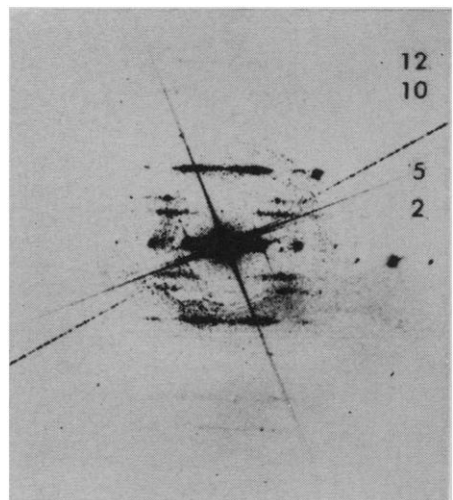


Fig. 2. Optical diffraction pattern of a longitudinal section through a chromatoid body. The indices l of the layer lines are indicated. The three long, thin lines passing through the pattern are artifacts.

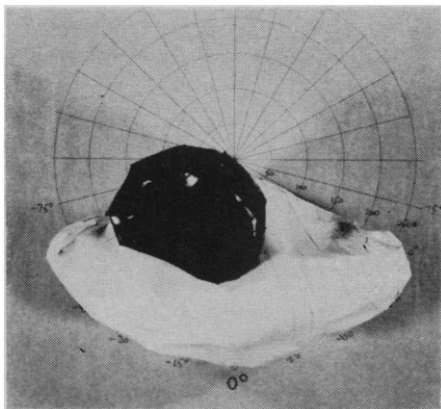


Fig. 3. Photograph of the shape (contours of zero electron density) of one ribosome of the helix. The helical axis passes through the origin of the polar coordinates, which give the scale of the model. Small subunit in black, large subunit in white.

subunit of any one ribosome is making contact across the helix axis with the central part of the large subunit of the next ribosome up the helix.

In order to interpret the diffraction pattern of Fig. 2, it was necessary to assign phases to the observed intensities. This has classically been done by assuming trial structures. Since previous work (1) had provided a clear interpretation of the helical packing of the ribosomes within these crystals, I felt that a trial structure consisting of "point" ribosomes placed on this helix required the fewest possible assumptions concerning the distribution of matter within any one ribosome, and would therefore afford the most general starting point. The chief restriction which this approach entails is that the resultant structure has a perpendicular dyad axis of symmetry. The model presented here is the first stage in the reconstruction of the structure of the ribosomes of chromatoid bodies.

RICHARD S. MORGAN

Department of Biophysics, Pennsylvania State University, University Park 16802.

References and Notes

1. R. S. Morgan and B. G. Uzman, *Science* **152**, 214 (1966).
2. I thank Dr. B. Uzman of the Children's Cancer Research Foundation, Boston, Mass., and her associates for this and other micrographs.
3. A. Klug, F. H. C. Crick, H. W. Wyckoff, *Acta Cryst.* **11**, 199 (1958).
4. D. De Rosier and A. Klug, *Nature* **217**, 130 (1968).
5. R. S. Morgan, H. S. Slayter, D. L. Weller, *J. Cell Biol.* **36**, 45 (1968).
6. M. L. Petermann, *The Physical and Chemical Properties of Ribosomes* (Elsevier, Amsterdam, 1964).
7. Supported in part by a departmental grant NsG-324 from NASA, I thank F. Kellogg for discussion.

27 August 1968

8 NOVEMBER 1968

Plant-Herbivore Coevolution: Lupines and Lycaenids

Abstract. Predation on lupine flowers by larvae of a lycaenid butterfly was studied by comparison of inflorescences exposed to and protected from infestation, and by comparison of lupine populations exposed to different degrees of attack. The lycaenids caused striking reduction in seed set, indicating that this small herbivore could act as a potent selective agent in lupine populations.

Coevolutionary interactions between plants and herbivores have been studied (1) and may be a major source of organic diversity (2). The selective effect of herbivore attack on plants, except the most extreme attacks which lead to extensive defoliation, are usually discounted as having little influence on plant populations. Also discounted is the primary role of plant biochemicals as herbivore poisons (3). Kemp (4) described an example of extreme selection for procumbency in pasture plants under heavy grazing. A seemingly insignificant herbivore, the small (wing length ± 14 mm) lycaenid butterfly *Glaucopsyche lygdamus* Doubleday, may have a profound effect on the reproductive capacity of the herbaceous perennial lupine *Lupinus amplus* Greene. This supports the contention that plants are under powerful evolutionary attack by herbivores, an attack not apparent to the casual observer.

Lupine populations in the vicinity of Gothic and Crested Butte, Gunnison County, Colorado, were investigated in June and July of 1968. Female butterflies oviposited only on pubescent portions of immature inflorescences of *L. amplus*. No oviposition was observed on an inflorescence in which some flowers were opened. A comparison of two inflorescence types, both of which occur on the same plants, was made on 7 July. Eggs and egg shells were counted on 125 inflorescences without open flowers (Fig. 1) and 130 inflorescences which had open flowers at the base only (Fig. 1). The unopened portion of the inflorescence presented an oviposition environment to a female butterfly which we are unable to distinguish from an immature inflorescence, except for the presence of opened flowers below, and increased distance from, the crown of the lupine plant. Table 1 shows the very significant difference ($P \ll .01$) in egg distribution on the two types of inflorescences. Note that since the eggs and egg shells remain attached after the flowers open, all of the eggs found at this time on open flowers may have been laid on the inflorescence when it was immature.

Larvae feed primarily on the wing and keel of the corolla and the stamens which are contained within the keel (54 of 78 larvae observed were feeding in these areas). Other parts of the flower, including the ovary, are less frequently attacked. Flowers attacked by lycaenids often do not reach anthesis and subsequently abscise.

One hundred immature inflorescences (of the type shown in Fig. 1) on 36 plants of the Gothic population were tagged on 5 July. Egg counts were made on all inflorescences and roughly half were designated controls. Controls either had no eggs on them, or had unhatched eggs removed. The tagged inflorescences were censused subsequently on 6, 9, 11, 14, and 17 July. Great care was taken not to damage the flowers. Periods between censuses were not long enough to permit egg hatch, so that we could, by removing all new eggs at each census, keep the controls free of attack by *G. lygdamus* larvae. On 17 July all inflorescences were collected and examined microscopically for damage. Floral scars were counted to give the total number of flowers which could have been produced on the inflorescence (potential production). At this date all inflorescences were fully mature and each flower had ovarian development. The lycaenid larvae found ranged in size from small (newly hatched) to large



Fig. 1. (Left) Inflorescence of *Lupinus amplus* without open flowers; (right) inflorescence with open flowers at base and unopened flowers at apex.